Moon-Based Ground Penetrating Radar Derivation of the Helium-3 Reservoir in the Regolith at the Chang'E-3 Landing Site

Chunyu Ding, Qingquan Li, Jiangwan Xu, Zhonghan Lei, Jiawei Li, Yan Su, and Shaopeng Huang

***Abstract*—The Moon-based ground penetrating radar (GPR) carried by the Yutu rover performed in-situ radar measurements to explore extraterrestrial objects, which provides an unprecedented opportunity to study the shallow subsurface structure of the Moon and its internal resources. Exploiting lunar resources might be one of the solutions to the Earth's energy shortage in the future. In this article, first, the thickness distribution of the lunar regolith at the Chang'E-3 landing site is derived using the high-frequency Yutu radar observation data. Second, the surface concentration of helium-3 is determined based on the surface TiO_2 content of the lunar regolith. Finally, the reservoir of helium-3 resources in the lunar regolith is estimated. Our result suggests that the helium-3 reservoir along the Yutu rover traveling route from the navigation points N105 to N208 ($\sim$445 m^2) is $\sim$37–51 g, and its helium-3 content per unit area is $\sim$0.083–0.114 g/m^2, which is at least five times higher than that of the global average. Currently, the nuclear fusion experiment is facing a severe shortage of tritium fuel. We discuss the possibility of replacing it with lunar helium-3 as the fuel for nuclear fusion. Meanwhile, we also suggest that the Chang'E-3 landing area can be a potential site selection for the exploitation of the lunar helium-3 in the future. Our results will provide a valuable reference to evaluate the economics and feasibility of mining in-situ helium-3 resources on the Moon.**

***Index Terms*—Chang'E-3 mission, Helium-3, lunar regolith, Moon-based ground penetrating radar (GPR).**

Manuscript received 31 December 2022; revised 13 February 2023; accepted 3 March 2023. Date of publication 7 March 2023; date of current version 23 March 2023. This work was supported in part by the National Natural Science Foundation of China under Grant 42241139 and Grant 42004099, in part by the Opening Fund of the Key Laboratory of Lunar and Deep Space Exploration, Chinese Academy of Sciences, under Grant LDSE202005, and in part by the Shenzhen Municipal Government Investment Project under Grant 2106-440300-04-03-901272. *(Corresponding authors: Chunyu Ding; Shaopeng Huang.)*

Chunyu Ding and Zhonghan Lei are with the Institute of Advance Study, Shenzhen University, Shenzhen 518960, China (e-mail: dingchunyu@szu.edu.cn; aleizhonghan@163.com).

Qingquan Li, Jiangwan Xu, and Shaopeng Huang are with the College of Civil and Transportation Engineering, Shenzhen University, Shenzhen 518060, China (e-mail: liqq@szu.edu.cn; 2060471033@email.szu.edu.cn; shaopeng@umich.edu.).

Jiawei Li is with the Lunar Exploration and Space Engineering Center, China National Space Administration, Beijing 100086, China (e-mail: lijiawei1228@sohu.com).

Yan Su is with the Key Laboratory of Lunar and Deep Space Exploration, National Astronomical Observatories, Chinese Academy of Sciences, Beijing 100049, China, and also with the School of Astronomy and Space Science, University of Chinese Academy of Sciences, Beijing 100049, China (e-mail: suyan@nao.cas.cn).

Digital Object Identifier 10.1109/JSTARS.2023.3253499

I. Introduction

THE Moon is the natural satellite of our Earth, and it is also the preferred target for human beings to explore extraterrestrial objects [1]. As the evolution terminal of terrestrial planets, investigation of the Moon can also help us better understand the future of our Earth [2]. So far, human beings have carried out more than 130 exploration missions to the Moon, with a success rate of about 50% [3]. Not only does the Moon have a large number of scientific problems awaiting further study, but also the resources to be exploited [1], [4]. For example, ilmenite, which is a mineral with a chemical composition of TiO_2 + FeO, is rich in basalt on the Moon, and there are huge amounts of potassium and uranium (e.g., the concentration of potassium and uranium are observed to be 500 μ g/g and 200 ng/g in mare basalt, respectively; [5]), rare Earth elements (REEs) in KREEP, and the helium-3 resources stored in the lunar regolith [4], [6]. KREEP is the lunar material having very high concentrations of incompatible elements, which is mainly composed of potassium (the atomic symbol is letter K), REEs, and phosphorus (the atomic symbol is letter P) [7]. The solar wind carries a large amount of helium-3 material blew into the lunar regolith (e.g., the Apollo samples laboratory measurements confirmed the existence of the helium-3 material stored in the lunar regolith [8]), which results in the estimated storage of the helium-3 reservoir over one million tons on the global Moon [4], [9], [10], [11], [12].

The fact that the lunar regolith contains the helium-3 is the result of laboratory measurements on Apollo samples [4], [14], [15]. Even though the laboratory measurements of Apollo samples exhibit that there is a very small concentration of helium-3 enriched in the lunar regolith with an average concentration of about 3.59 ppb [14], it is still triggered a great interest for scientists [16]. The discovery of the lunar helium-3 resources, which is a candidate material for nuclear fusion and may provide new supplies for future Earth's energy shortage [17], [18], [19], [20]. The total helium-3 reservoir in the entire Moon is strongly associated with the thickness of the lunar regolith [11]. Assuming that the concentration of helium-3 in the lunar regolith is a homogeneous distribution with depth, Swindle et al. [14] estimated that the helium-3 reservoir in the global of the Moon is 3.22×10^9 kg. On the other hand, it is assumed that the concentration of helium-3 in the lunar regolith decreases with depth. The total content of the helium-3 was calculated to be $\sim 6.6 \times 10^8$ kg on the entire Moon by the Chinese Chang'E-1

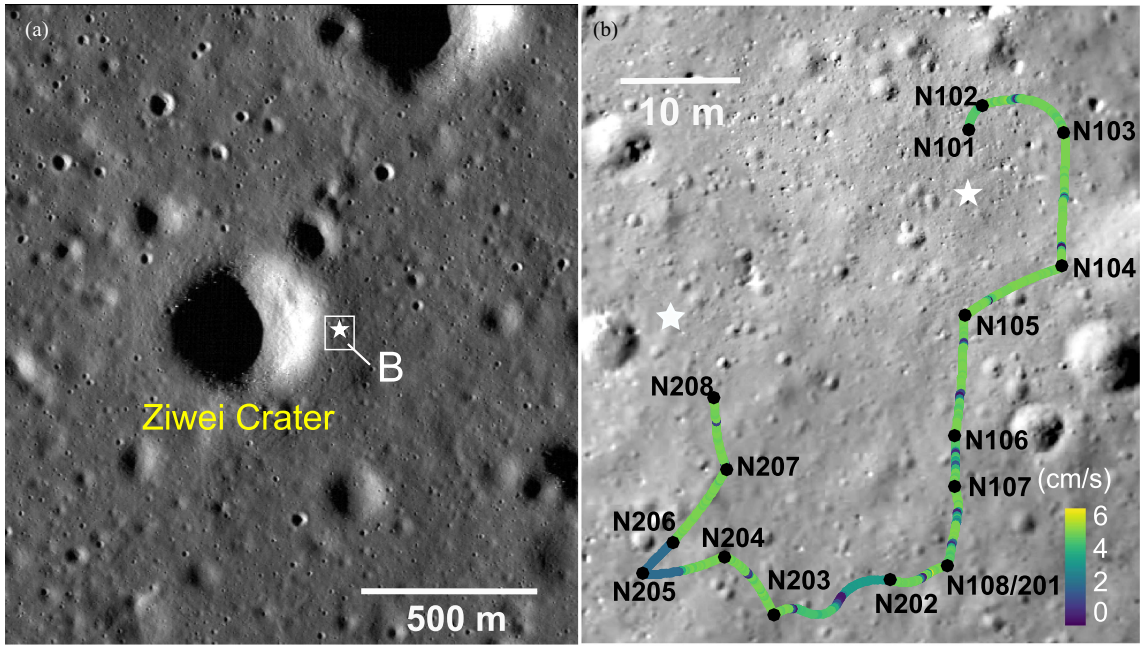

Fig. 1. (a) Geological context of the Chang'E-3 landing site, the white star indicates the location of the lander. The base image is acquired from LROC NAC (image ID: M102285549LE). (b) Yutu rover traveling route within the first two lunar days on the Moon's surface. The black dots represent different navigation points, and the different colors on the traveling route represent the speed of the Yutu rover, which has an average speed of ∼5.5 cm/s [13]. The base image is acquired by the descent camera of the Chang'E-3 lander with the image ID of CE3_BMYK_LCAM-3006.

microwave radiometer observation [11], [18]. According to the above remote sensing results, the total helium-3 reservoir in the whole Moon is at least 660 000 tons, but the total reservoir of that on Earth is only 20 tons [11]. Simko et al. [19] hypothesized that one million tons of the helium-3 can supply the energy needs of our Earth for at least 5000 years. All of the above discuss the helium-3 resources on a global scale, but the reservoir of in-situ helium-3 estimation has not been reported. The estimation of the global helium-3 reservoir is observed by space-borne instruments, e.g., Clementine's spectrometer and the Chang'E-1 microwave radiometer [9], [18]. However, these space-borne instruments usually have a low spatial resolution, e.g., the Chang'E-1 microwave radiometer has a spatial resolution of 30–50 km [18]. Thus, it is unable to precisely detect the thickness of the lunar regolith in a small-scale region (e.g., the Chang'E-3 landing site), so the indirectly obtained helium-3 resources in a small-scale region are not precise enough. However, the Moon-based ground penetrating radar (GPR) onboard the Yutu rover provides a possibility to estimate the thickness of the lunar regolith with a high resolution in the small-scale region.

In this article, the in-situ helium-3 reservoir is first indirectly estimated by the Yutu high-frequency radar at the Chang'E-3 landing site, and we also discussed its economic benefits and potential future applications. The general structure of the article is as follows: First, we introduce the Yutu radar system and the data collection on the Moon, see Section II-A. Second, the quantitative estimation approach of the helium-3 reservoir is derived in Section II-B. Third, the distribution of the regolith thickness along the Yutu rover traveling path is estimated using the high-frequency Moon-based GPR data (see Section III-A), and then, the surface concentration of helium-3 at the landing site is determined by the function of the TiO_2 content and the helium-3 concentration (see Section III-B). Fourth, the reservoir of helium-3 in the lunar regolith is estimated (see Section III-C). Finally, we discussed the content and origin of helium-3 (see Sections IV-A and IV-B), its economic benefits and possible future applications have also prospected see Section IV-C, and we also discuss the proposal of the Chang'E-3 landing site as a potential mining area for the helium-3, see in Section IV-D.

II. Radar, Data, and Method

A. Yutu Radar Descriptions

In 2013, the Chang'E-3 mission has been successfully landed in the northeastern Mare Imbrium on the near side of the Moon, with a latitude and a longitude of 44.1260°N, 19.5014°W [23], [25]. The Chang'E-3 lander [see Fig. 1(a), the white star] is located ∼50 m away from the eastern rim of the Ziwei crater, which has a diameter of ∼450 m, shown in Fig. 1(a); [26], [27]. The landing site is located on the top of the Eratosthenian-aged basalt whose absolute model age is constrained to be ∼2.5 Ga [23], [27]. The Yutu rover traveled a total of ∼114 m on the surface of the Moon [23], and its traveling speed is not uniform [e.g., different colors in Fig. 1(b)], which has an average speed of ∼5.5 cm/s [21], [28].

The Moon-based GPR carried by the Yutu rover is the first in-situ radar instrument operation on the surface of the Moon, which provides an unprecedented opportunity to study the lunar subsurface structure and its potential in-situ resources [21], [23], [25], [29], [30]. The Yutu radar consists of low-frequency and high-frequency channels, respectively [29]. The low-frequency and

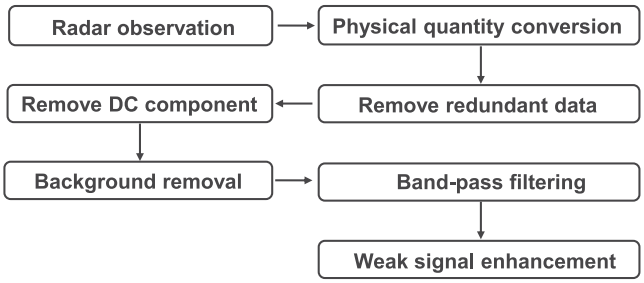

Fig. 2. Data processing flow of the Moon-based high-frequency GPR radargram.

high-frequency Moon-based GPR channels are installed at the rear and on the bottom of the Yutu rover, respectively [29]. The operating frequency of the low-frequency channel is 60 MHz, and its frequency ranges from 40 to 80 MHz [29]. The depth resolution of the low-frequency channel is ∼1 m [23], [29] in the regolith-like material, and it is mainly used to detect subsurface structures of the Moon with a penetration depth greater than 100 m [29]. The high-frequency channel works at an operating frequency of 500 MHz, and its frequency ranges from 250 to 750 MHz [31]. The depth resolution of the high-frequency channel is better than 0.3 m validated by the ground experiment in the simulated lunar regolith [31], whose relative permittivity is measured to be ∼2.89 in the field [32]. The high-frequency channel is composed of three butterfly antennas separated by a distance of ∼0.16 m [29], one of which transmitter and the other two receivers. The time window is designed to be 640 ns, which is mainly used to probe the thickness and the interior structure of the lunar regolith [25], [29]. Since the low-frequency Moon-based GPR system is insufficient to detect the thickness of the lunar regolith layer [23], [24], [33], only the high-frequency Moon-based GPR observation data are used in this article.

B. Data Collections

Although the Yutu radar has a survey line of ∼114 m on the surface of the Moon [23], [28], the data between the navigation points N208-N209 was lost, so it is a total of ∼107.4 m radar observation data obtained [21]. The radar data adopted in this study can be freely downloaded from the Lunar and Planetary Data Release System (http://Moon.bao.ac.cn). The high-frequency radar data need to be preprocessed to improve the signal-to-noise ratio before it can be effectively used for further research. This article adopts the conventional data preprocessing methods for the Yutu radar observation data [21], e.g., background removal, band-pass filtering, and weak signal enhancement. The data processing flow of the Moon-based GPR observation data is shown in Fig. 2, and the processed radargram is shown in Fig. 3(a). It is worth noting that because the radar is in the debugging stage between the navigation points N101 and N105, multiple sets of different gain parameters are set, resulting in discontinuity of the radargram [21], [28]. The radar measurement after the navigation point N105 are all set with the same parameter (e.g., 0 dB gain; [21]). Therefore, this study only used the radar data from the navigation points N105 to N208 to unify the data, which corresponds to ∼74.2 m in distance along the radar survey line.

The first layer is at a depth of ∼0.74 m, shown as the yellow dashed line in Fig. 3(b). The amplitude of the radar echoes changes from weak to strong, indicating the difference of the material in the subsurface of the Moon, and it can be inferred as the interface between the fine-grained regolith and the underlying ejecta material of the Ziwei crater. The second layer is at a depth of ∼4.3 m, shown as a red dashed line in Fig. 3(b). The amplitude of the radar echoes changes from strong to weak, which is inferred as the interface between the ejecta material and the paleo-regolith. The third layer is at a depth of ∼9.3 m, shown as a green dashed line in Fig. 3(b). The amplitude of the radar echoes gradually approaches the noise level, which is inferred as the interface between the paleo-regolith and its underlying materials.

C. Method for Estimating the Helium-3 Reservoir

The helium-3 reservoir in the lunar regolith is mainly associated with the direct injection of the solar wind, and its concentration adheres to the surface of its particles. The lunar regolith is a layer of loose material covering the bedrock of the entire Moon [34], and its formation and thickness mainly depend on the frequency of the bombardment of impacts [1]. The physical process of binding helium-3 to the lunar regolith is the implantation of the solar wind. The average speed of the solar wind on the lunar surface is ∼468 km/s [35], and the average energy of helium ions is ∼4 keV in the solar wind [36]. Although the thickness of the helium-3 implanted by the solar wind is ∼1 mm in the lunar regolith [37], the diffusion process of the helium-3 actually implanted into the lunar regolith takes a long time to reach equilibrium [36]. Therefore, the concentration distribution of helium-3 in the lunar regolith is deeper than that of the solar wind implantation. The lunar surface is frequently impacted by meteorites of different sizes, and the deep lunar regolith will be excavated and overturned [34] and re-exposed on the lunar surface to receive the helium-3 implantation. Therefore, the concentration of helium-3 in the lunar regolith may be evenly distributed along the vertical depth. In addition, ilmenite has stronger adsorption on the helium-3 compared with other lunar minerals (e.g., the content of helium-3 in ilmenite is 10–100 times than that of other minerals [11], [38]). The crystal of ilmenite has a hexagonal close-packed structure, and its lattice spacing is similar to the size of helium-3 atoms, so it is easy to capture the helium-3 atoms [36]. The majority of TiO_2 in the lunar regolith is hosted by ilmenite, and the content of TiO_2 can be used as an indicator of the helium-3 retention capacity of the lunar regolith [11].

To estimate the helium-3 reservoir of the lunar regolith, we first need to know its thickness and the surface concentration of helium-3. Then, the total helium-3 reservoir in a specific area can be obtained by calculating the volume of the lunar regolith by multiplying the concentration of helium-3 along with the depth. The volume of the lunar regolith can be measured by the high-frequency Moon-based GPR. The concentration of helium-3 can be obtained from the laboratory measurement of Apollo regolith samples. Previous studies have shown that the concentration of helium-3 in the lunar regolith is directly related

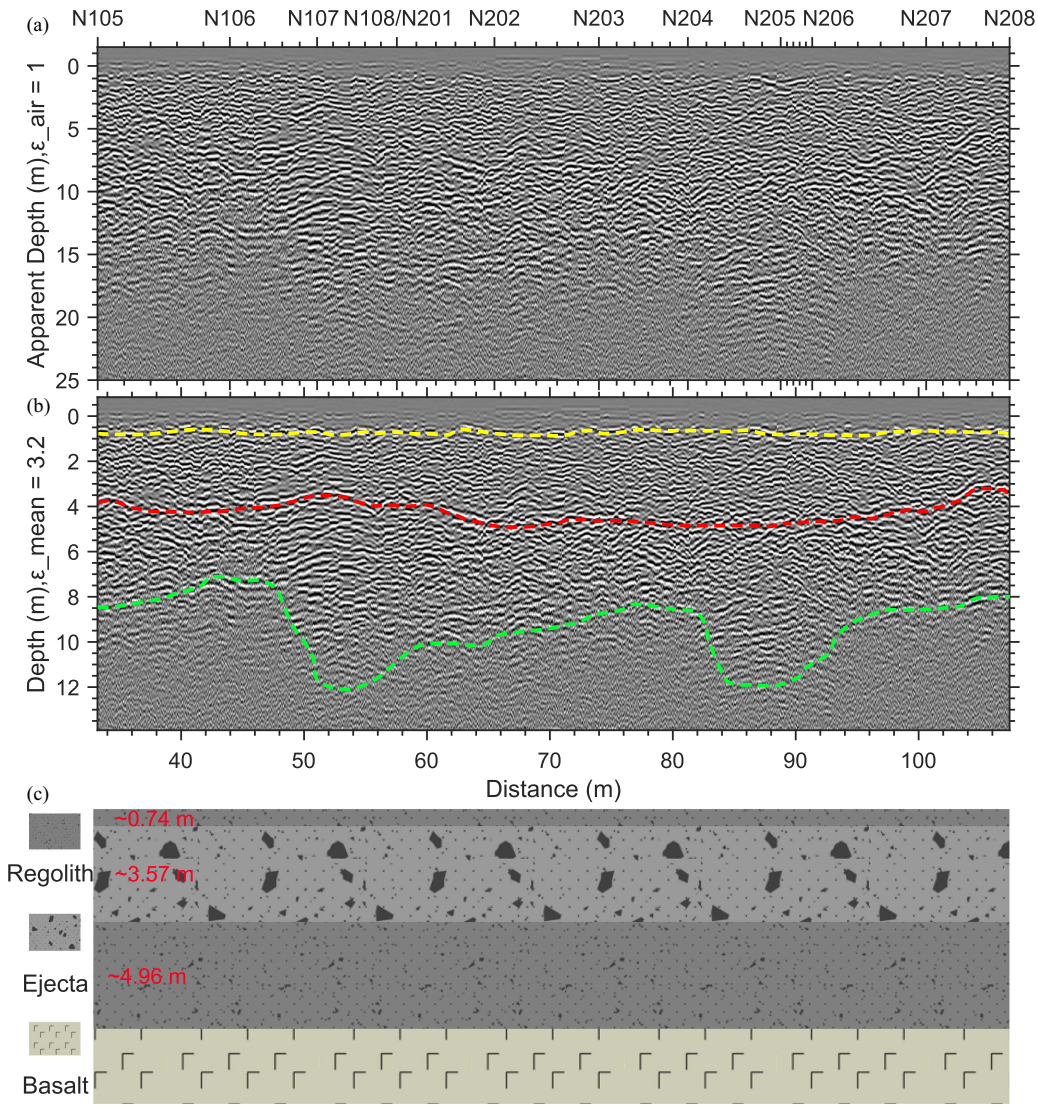

Fig. 3. Radargram acquired by the high-frequency Moon-based GPR at the Chang'E-3 landing site, and its schematic diagram of geological interpretation. 0 is the surface ground of the Moon on the Y-axis. (a) Raw 2B-level radar data has been processed by background removal, band-pass filtering, and weak signal enhancement. It is worth noting that the intensity contrast of the amplitude in the radargram is destroyed after weak signal enhancement, but it does not affect the interpretation. The left axis is the apparent depth, which corresponds that the relative permittivity of the subsurface material is assumed to be 1. (b) Processed radargram. The left axis is converted to depth by the relative permittivity of the lunar regolith calculated to 3.23 [21], [22]. The yellow dashed line indicates a layer of the fine-grained lunar regolith [23], [24]. The red dashed line draws the interface of the regolith-like ejecta and the paleo-regolith [22]. The blue dashed line marks the layer of paleo-regolith [23]. (c) Geological profile of the interpretation at the Chang'E-3 landing site with a depth of ∼10 m. The fine-grained lunar regolith is ∼0.74 m thick, the regolith-like ejecta has a thickness of ∼3.57 m, and the thickness of paleo-regolith is ∼4.96 m.

to its TiO_2 content [11], [14]. However, previous studies have also shown that as the depth increases, the deep lunar regolith being excavated is relatively infrequent by the impacts, so the helium-3 being implanted by the solar wind is mitigated [11], [14]. It caused the depth profile of the concentration of helium-3 content to be not homogeneous in the lunar regolith. Laboratory simulation results show that the distribution of the concentration of helium-3 exhibits an exponential decay trend with increasing depth [11], [39] so that the total helium-3 reservoir in the lunar regolith can be calculated by

$$M = \int_0^x \int_0^y \int_0^z \rho(z) \cdot C_0 e^{-\frac{z}{\gamma}} dxdydz \tag{1}$$

where x, y is the spatial position (m), z is the observed thickness of the lunar regolith (m); $\rho(z)$ is the density (kg/m^3) of the lunar regolith; C_0 is the surface concentration of helium-3, whose unit is ppb, 10^{-9} g/g [15]; γ is the scale of attenuation (m). The technical process for estimating the helium-3 reservoir in the lunar regolith in detail is shown in Fig. 4.

III. Results

A. Thickness Distribution of the Lunar Regolith Along the Yutu Rover Traveling Path

The Moon-based GPR radargram is composed of the amplitude of the signal and the two-way traveling time. To transfer the time to depth in the radargram, it is necessary to calculate the

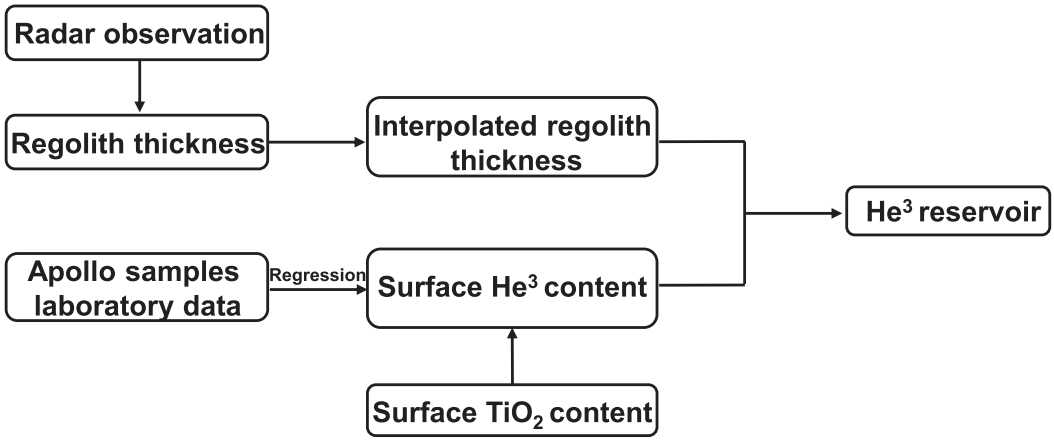

Fig. 4. Technical process for estimating in-situ helium-3 reservoir of the lunar regolith at the Chang'E-3 landing site.

speed of the radar pulse propagating in the subsurface material, which can be calculated by the following formula:

$$d = \frac{c}{\sqrt{\varepsilon}}\tau \tag{2}$$

where c is the speed of electromagnetic wave propagation in free space, 3×10^8 (m/s); ε is the relative permittivity of the lunar subsurface material; τ is the one-way traveling time (ns). The propagation speed of the Moon-based GPR pulse in the lunar regolith is constrained to be ∼0.17 m/ns by the hyperbolic fitting method [21]. The depth information of the radargram after conversion is shown in Fig. 3(b).

The area detected by the Yutu radar is on the top of the continuous ejecta blanket of the Ziwei crater [23]. A fine-grained lunar regolith about 0.74 m thick developed on the continuous ejecta blanket of the Ziwei crater after 26.7 Ma [see Fig. 3(b) and (c)]; [23], [24]. Radar echoes exhibit sharp changes at depth of ∼4.2 m, indicating the interface of the ejecta blanket underlying the paleo-regolith, dashed red line in Fig. 3(b) [21]. The relative permittivity of the ejecta blanket is estimated to be ∼3.23 [21], which is consistent with that of the typical lunar regolith of Apollo samples [34]. This suggests that the continuous ejecta blanket ($<$ 4.2 m) of Ziwei is made of regolith-like materials. The reason is that while the Ziwei crater was formed, its excavation depth may be ∼11 m [40] not ∼34 m [41], and the median thickness of the surface regolith before the Ziwei crater was inferred to ∼8 m [42]. The ejecta blanket was formed by excavating the underlying bedrock and reversal of the surface lunar regolith during the impacting process [41]. Therefore, we speculate that the ejecta blanket is composed of the regolith mixture with rock fragments but still dominated by the regolith. The percentage of the regolith in the ejecta is estimated to be ∼70%–93% [43]. Most of the regolith in the ejecta is formed by the overturning of the paleo-regolith during the formation of the Ziwei crater, so we assume that the distribution of helium-3 in the ejecta is equivalent to that of paleo-regolith. Radar echoes at a depth $>$ 4.2–10 m are considered to be the lunar regolith before Ziwei, that is paleo-regolith (see Fig. 3(c); [23]). Therefore, this article suggests that the subsurface materials detected by the Chang'E-3 high-frequency radar within the depth of ∼10 m can be considered as the lunar regolith (see Fig. 3). It is generally believed that the regolith thickness is ∼5 m in the Mare region and $>$10 m in the highland region on the Moon [44]. Therefore, our estimated result is double the average thickness of the lunar regolith in the Mare region. The thickness of the lunar regolith observed by the Yutu radar varies from ∼7.43 to 11.34 m, with an average thickness of ∼9.24 m [see Fig. 3(c)], and then, it is projected onto the Yutu rover traveling route from navigation points N105 to N208 [see Fig. 1(b)]. The thickness distribution of the lunar regolith between N105 and N208 is interpolated through the method of the neighbor interpolation [45]. The interpolated area between N105 and N208 is estimated to be ∼445.00 m^2 shown in Fig. 5.

B. Constraint of the Surface Concentration of Helium-3

The regolith of the different geological units receives the various degree of helium-3 implanted from the Sun, which leads to the spatial inhomogeneity of the surface concentration of helium-3 (C_0) on the Moon. The value of C_0 depends on the flux of the solar wind reaching the lunar surface, the optical maturity of the lunar regolith (OMAT), and the content of TiO_2 of the regolith [11]. In general, the lunar regolith maturity and OMAT are strongly associated with the age of the geological unit, and there are more helium-3 adsorbed on the surface particle of the fine-grained regolith. However, the variation of helium-3 content in the lunar regolith has a significant correlation with the local TiO_2 content, rather than OMAT [11], [18]. Therefore, even though the lunar regolith is not mature (e.g., the regolith of the Chang'E-3 landing site; [46]) but the high TiO_2 content may also lead to a high helium-3 reservoir. By measuring Apollo regolith samples collected in the different geological units (e.g., Apollo 12, 14, 15, 16, and 17 sites; [38]), the function of the concentration of helium-3 and TiO_2 content is obtained shown in Fig. 6. The regression analysis is performed on the measured data, and a linear regression equation is obtained as

$$y = 1.072x + 1.379 (R^2 = 0.81) \tag{3}$$

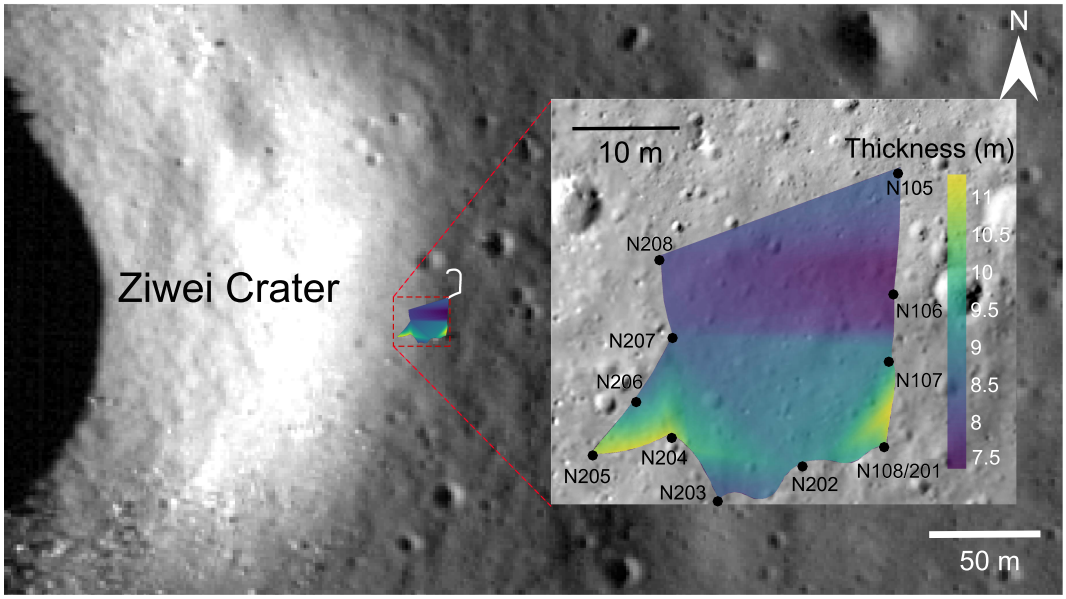

Fig. 5. Thickness distribution of the lunar regolith and the Ziwei crater at the Chang'E-3 landing site. The colors in the inserted image represent the thickness variation from N105 to N208. The spatial distribution of the lunar regolith thickness was obtained by neighbor interpolation [45].

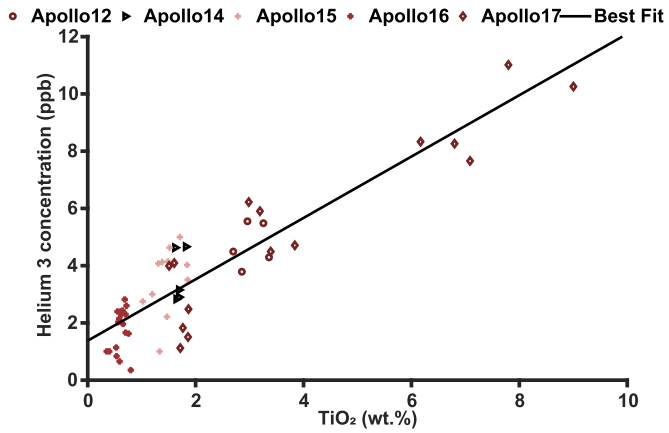

Fig. 6. Relationship between TiO_2 (wt.%) content and the concentration of helium-3 (ppb, 10^{-9} g/g). The data are from the laboratory measurement of Apollo regolith samples [38].

where y is the concentration of helium-3 (ppb, 10^{-9}g/g), and x is the TiO_2 content (wt.%).

The surface TiO_2 content is measured by the in-situ APXS (Active Particle-induced X-ray Spectrometer) and VNIS (Visible and Near-infrared Imaging Spectrometer) multiple times along the Yutu rover traveling path at the Chang'E-3 landing site [47]. The estimated surface TiO_2 content has a range from ~4.6 wt.% to 5.2 wt.% with an average of ~5.0 wt.% [47], and the discrepancy of the composition of the surface regolith in the spacial distribution may be associated with uncertainty. The average surface concentration of helium-3 at the Chang'E-3 landing site can be constrained to 6.74×10^{-9} g/g by substituting ~5.0 wt.% of TiO_2 content into the empirical formula (3). It is worth noting that the instruments of APXS and VNIS cannot penetrate into the lunar regolith so the depth profile of the helium-3 concentration within the ilmenite is unknown. In this article, we adopt two hypotheses to estimate the mass of the helium-3 in the lunar regolith, which are as follows: 1) the helium-3 concentration within the ilmenite along the vertical depth is homogeneous, and 2) the helium-3 concentration is in-homogeneous.

C. Total Helium-3 Reservoir Estimated by the Yutu Radar Measurements

After obtaining the thickness distribution of the lunar regolith along with the Yutu rover traveling route (see Section III-A) and the surface concentration of helium-3 (see Section III-B), the total helium-3 reservoir can be estimated by substituting these two parameters into (1). The concentration of helium-3 inside the lunar regolith is assumed nonuniformly distributed along with the depth, which is controlled by the scale of attenuation (γ). In the previous studies, γ is commonly assumed to be 3 m for estimating the helium-3 reservoir of the whole Moon [11], [14], [39], and we assume that the scale of attenuation (γ) obtained in the laboratory is a constant value. The physical properties of the lunar regolith at the Chang'E-3 landing site were estimated by the high-frequency Moon-based GPR in our previous studies [21], [22]. The velocity of the radar pulse propagation into the lunar regolith is estimated by the method of hyperbola fitting [see Fig. 7(a)], and then, it is converted to the relative permittivity distribution [see Fig. 7(b)] using the empirical equation from the data obtained by the Apollo samples measurements [49]. The depth profile of density in the lunar regolith increases with depth [50]. Similarly, we adopted the depth profile of density at the Chang'E-3 landing site from Fig. 7(c), and the depth-density equation is shown as follows:

$$\rho(z) = 2.35\frac{z^2 + 0.66z + 0.23}{z^2 + 0.66z + 0.47} \tag{4}$$

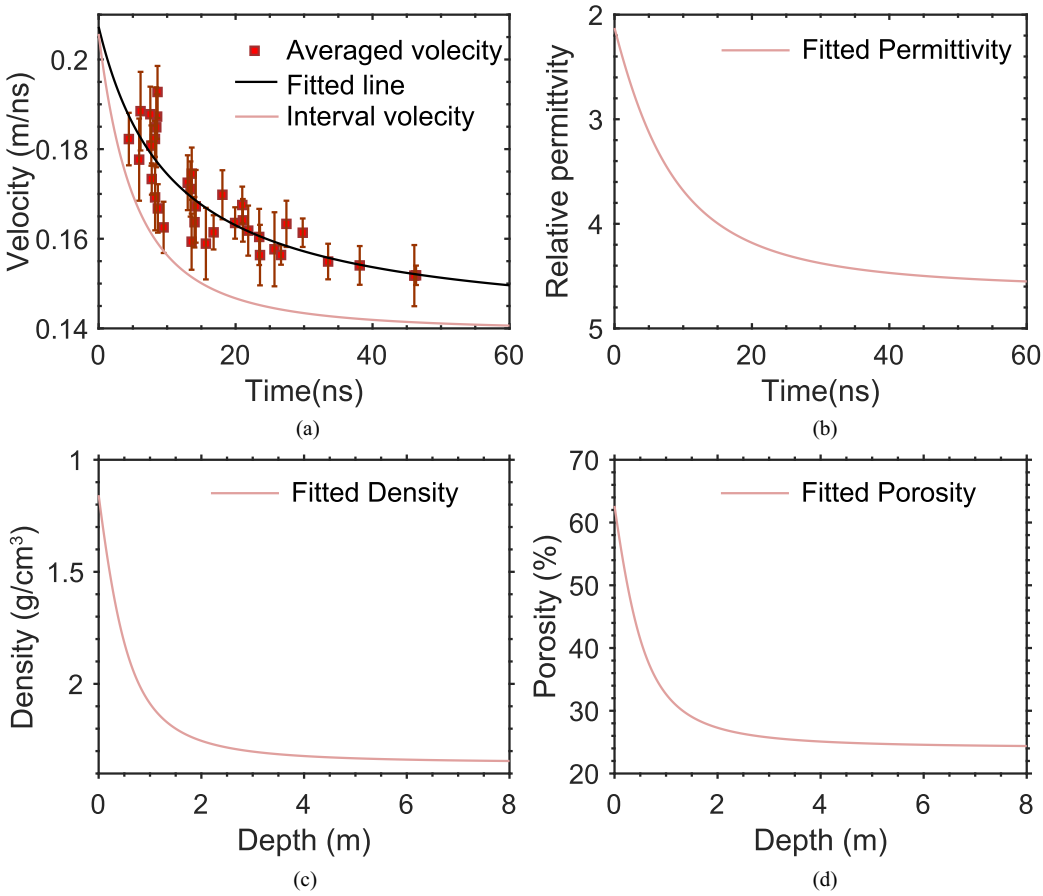

Fig. 7. Physical proprieties of the lunar regolith estimated by the high-frequency Moon-based GPR onboard Yutu rover [21]. (a) Radar pulse velocity propagation in the lunar regolith with time. The red dots represent the averaged velocity estimated by the Yutu radar, and the back line is the best-fitted averaged velocity. The light pink line is the interval velocity (v') conversion from the averaged velocity using the equation, $\sqrt{\frac{t_n v_n^2 - t_{n-1} v_{n-1}^2}{t_n - t_{n-1}}}$, where v is the averaged velocity, and t is the time. (b) Relative permittivity (ε) of the lunar regolith derived from the equation, $(\frac{c}{v'})^2$, where c is the velocity of the electromagnetic wave propagation in a vacuum. (c) Depth profile of the interval density (ρ) of the lunar regolith derived by the equation, $log_{1.919}(\varepsilon)$. (d) Depth profile of the porosity (n), which is derived by the equation, $1 - \frac{\rho}{\rho_{\text{grain}}}$, where ρ_{grain} is grain density, which is generally defined to be $\sim$3.1 g/cm^3 [48].

where z is the thickness of the lunar regolith (m). The porosity of the surface regolith [see Fig. 7(d)] within the top thickness of $\sim$0.3 m is constrained to be $\sim$44.69% at the Chang'E-3 landing site [21]. The content of TiO_2 on the surface of Chang'E-3 landing area is estimated to be 4.6 wt.% to 5.2 wt.% [47], which is used as the upper and lower limit of uncertainty. According to (1), we estimate the mass distribution of helium-3 content in the lunar regolith as shown in Fig. 8. Then, integrating the entire radar measurement area ($\sim$445.00 m^2) yields a total helium-3 reservoir of $\sim$ 37$\pm$2 g.

IV. Discussions

A. In-Situ Helium-3 Reservoir of the Lunar Regolith

The total content of the lunar regolith helium-3 in the area of $\sim$445 m^2 yields $\sim$ 37$\pm$2 g, and its corresponding helium-3 content per unit area is 0.083 g/m^2. It is $\sim$5 times higher than the average helium-3 per unit area estimated by Fa et al. [11] on the global scale (e.g., 0.017 g/m^2) but slightly lower than the estimated by Swindle et al. [14] (e.g.,0.085 g/m^2). The helium-3 reservoir estimated by Fa et al. [11] considered the distribution of helium-3 concentration in the lunar regolith to be in-homogeneous, but Swindle et al. [14] considered it to be homogeneous. If we assume that the concentration of helium-3 and density along the depth is also a homogeneous distribution in the lunar regolith at the Chang'E-3 landing site, (1) can be rewritten as the following:

$$M_{ho} = \rho \cdot C_0 \cdot V \tag{5}$$

where ρ is the average density of the lunar regolith (kg/m^3) and V is the volume of the lunar regolith (m^3). The results of previous studies show that the average density of the lunar regolith at the Chang'E-3 is estimated to be 1820 kg/m^3 [21], [22]. The surface concentration of helium-3 (C_0) is 6.74 $\times$ 10^{-9} g/g according to Section III-B. Then, we substitute those parameters into (5) to estimate the mass of helium-3 as shown in Fig. 8(b). Integrating the measurement area [see Fig. 8(b)] yields a total helium-3 reservoir of $\sim$ 51$\pm$2 g, corresponding to $\sim$0.114 g/m^2 per unit area, which is higher than that of Swindle et al. [14] as well.

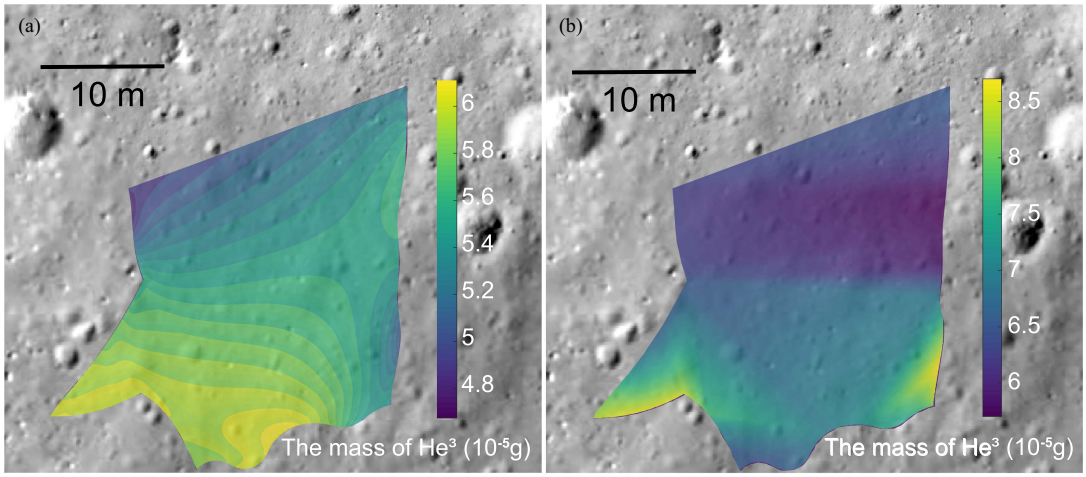

Fig. 8. Distribution of the helium-3 content along the Yutu radar traveling route from N105 to N208, and each pixel is 0.01 m. (a) Result of an inhomogeneous distribution of the helium-3 content in the lunar regolith. (b) Result of an homogeneous distribution of the helium-3 content in the lunar regolith.

In addition, the concentration of helium-3 from Apollo laboratory measurements may be underestimated [4], [15]. Schmitt et al. [4] argued that Apollo samples might lose a portion of their concentration of helium-3 due to unavoidable agitation during sample collection and transportation return to Earth before being measured. It believes that the concentration of helium-3 in the samples may be underestimated by as much as 40% [4]. Since the development of the lunar regolith is frequently through multiple impacts and overturns [34], the probability of helium-3 implantation into the lunar regolith is homogeneous to some extent reasonable, and its concentration does not decay with the increase of depth. Therefore, in the case of an inhomogeneous distribution, and considering the possible loss of transportation agitation, the helium-3 reservoir per unit area should be re-calculated to be $\sim$0.138 g/m^2, which can be treated as a lower limit. In the case of a homogeneous distribution, and considering the possible loss of transportation agitation, the helium-3 reservoir per unit area of the Chang'E-3 landing site should be recalculated to be $\sim$0.190 g/m^2, which can be treated as an upper limit.

B. Origin of the In-Situ Helium-3 Resources

The helium-3 of the lunar regolith is the result of long-term and continuous implanting of the solar wind [4], [9], [10]. Several factors influence the storage capacity of helium-3 in the regolith, e.g., the maturity of the regolith, the adsorption of helium-3 by the surface of the regolith particle, and the content of different minerals in the regolith, and the physical properties of the regolith [11]. It is generally believed that the capacity of the helium-3 retention to the particle interior of the regolith strongly relates to its exposure time on the Moon's surface. The maturity of regolith can usually be quantitatively characterized by the OMAT. The OMAT value of regolith at the Chang'E-3 landing area is observed to be $\sim$0.147 by the space-borne instrument [51], indicating that it is immature. This is consistent with the radar observation of the lunar subsurface material and the presence of a large number of rock fragments at the Chang'E-3 landing site [21]. Because the interior regolith of the Chang'E-3 is immature, it reflects that its plowing rate is slow, and the helium-3 implanted by the solar wind may be lower than that in other mature regions. However, minerals within the regolith also affect the adsorption of helium-3, especially the ability of TiO_2 to adsorb helium-3 is 10 to 100 times than that of other minerals (e.g., pyroxene, olivine, and plagioclase; [11], [18]). The TiO_2 content on the surface regolith is estimated to be $\sim$5.0 wt% using the in-situ Yutu APXS and VNIS data [47], which is higher than the global average value. The TiO_2 + FeO content inside the regolith of the Chang'E-3 is constrained to be $\sim$26% [13], which is also higher than the global average value. Therefore, we infer that although the regolith is not mature enough, its internal TiO_2 content is high, showing a strong helium-3 retention capacity at the Chang'E-3 landing site.

C. Economic Benefits of the Helium-3 Resources

The total storage of helium-3 resources at the Chang'E-3 seems considerable, but the storage per unit volume is likely scarce. If the in-situ helium-3 resources in the lunar regolith are thought to exploit in the future, which is whether the expected economic benefits can be achieved or not, it is an urgent problem to be solved. As follows, we will discuss the possible cost and value of the exploitation of the in-situ helium-3 on the Moon, and the possibility of replacing tritium with helium-3 for nuclear fusion.

1) Possible Cost of Exploitation of the In-Situ Helium-3 Resources: The helium-3 resources on Earth are rare with an estimated reservoir of $\sim$20 tons [52], but the helium-3 resources on the Moon are very abundant with a reservoir of over one million tons [11], [53]. If the in-situ helium-3 resources on the lunar surface are intended to be exploited commercially in the future, the economic input–output ratio needs to be considered to achieve the purpose of profitability. Schmitt et al. [4] estimated the total cost of stationing a complete mining system (including the fee of research and development, launch and return, personal costs, equipment, base delivery materials, etc.) for exploiting the

lunar helium-3 resources would cost 17 billion US dollars [19]. However, we consider that it may underestimate the cost of the construction of the helium-3 mining system on the lunar surface.

A more possible and feasible proposal for the lunar helium-3 mining system is introduced by Kleinschneider et al. [54], currently. The cost of the Earth–Moon transfer transportation and mining equipment construction on the Moon's surface are considered in their proposal, e.g., 22 orbital transfer cargo fleets, 3 lunar ascent/descent vehicles, and 1700 to 2000 Mark III helium-3 mining machines of the University of Wisconsin are proposed to be deployed on the Moon's surface [54]. The cost of exploiting 2 tons of the helium-3 per year should spend between \$7.7 billion to \$20.5 billion, and exploiting 20 tons of the helium-3 needs to cost between \$45.6 billion to \$140.3 billion per year. It is worth noting that the monetary unit in Kleinschneider et al. [54] is the euro. This article is calculated by converting the exchange rate into US dollars on September 19, 2022, whose rate of euro to US dollar is approximately 1:1. Taking the production of 2 tons of the helium-3 per year as an example, the production cost per gram of the helium-3 is estimated to be \$3850/g to \$10 250/g [54]. However, the current commercial cost of He-3 exceeds \$20 625/g (price in 2020) [55]. It is worth noting that the lunar helium-3 mining system proposed by Kleinschneider et al. [54] does not completely cover all possible input costs, and the cost proposed in their paper does not consider currency inflation after a few decades later.

We should emphasize that it is a very complicated systematic project to establish a large-scale helium-3 mining system on the Moon starting from scratch. It is necessary to consider not only the investment of equipment, but there are the structural design of mining base construction (e.g., designing the overall structure of a lunar mining base), operation engineering and infrastructure (e.g., transportation of materials and equipment to the Moon in the early stage of construction, deployment of mining machinery, and completion the construction of mining base by the automatic robots, etc.), settlement construction for human on the Moon (e.g., the mining system of the Moon cannot all be handed over to robots. There is still a need for the human to participate, which may require the establishment of human settlements and services), the design of automatic equipment (e.g., the design of various types of mining robots, maintenance robots, mineral transportation machinery, and spacecraft for transferring cargo between the Moon and Earth, etc.), and the construction of networks for controlling various automation systems for the mining base on the Moon. In addition, it is also necessary to consider and make a plan for the possible risks, e.g., the Moon has no atmosphere, the gravity is only one-sixth that of Earth, and the lunar regolith is composed of fine and loose materials, so it inevitably leads to dust raising and blocking mining machines and equipment during the process of mining. Therefore, it is necessary to develop mining machines and equipment to prevent the blockage of lunar dust ahead of exploiting the helium-3 on the Moon.

In general, the transportation cost of extraterrestrial mining plays an important role [55]. However, with the development of space transportation for decades, especially with more private companies such as SpaceX participating in space transportation, we believe that the transportation cost between Earth and the Moon will be much reduced in the future.

2) Helium-3 on the Moon: Substitute to Tritium?: The shortage of tritium fuel may lead to the stagnation of nuclear fusion development [56]. Helium-3, which is also used as a fusion fuel, may be considered as a substitute to promote the development of nuclear fusion reactors. Tritium and helium-3 can be produced by D+D (deuterium and deuterium) nuclear reactions on Earth under different temperatures, and the reaction equations are as follows [57]:

$$\mathrm{D} + \mathrm{D} \rightarrow \mathrm{n}(2.45\mathrm{MeV}) + {}^3\mathrm{He}(0.817\mathrm{MeV})$$
$$\mathrm{D} + \mathrm{D} \rightarrow \mathrm{p}(3.02\mathrm{MeV}) + \mathrm{T}(1.01\mathrm{MeV})$$

where n is the released neutron; p is the released proton. Nuclear fusion in development is mainly a reaction composed of D+T (deuterium and tritium) reaction [56]. The cost of production of tritium by the D+D reaction is very expensive. For example, it takes two billion US dollars to produce 1 kg tritium, that is, the cost price is \$2 million/g, which is an unbearable economic investment [56].

Tritium nuclear fusion is a reaction of deuterium and tritium (D+T), which produces a neutron (releasing 14.1 MeV) and a helium-4 (releasing 3.5 MeV), with releasing total energy of 17.6 MeV. The fusion equation is expressed as [57]

$$\mathrm{D} + \mathrm{T} \rightarrow \mathrm{n}(14.1\mathrm{MeV}) + {}^4\mathrm{He}(3.5\mathrm{MeV}).$$

The helium-3 nuclear fusion is a reaction of deuterium and helium-3 (D+He-3), which produces a proton (releasing 14.68 MeV) and a helium-4 (releasing 3.67 MeV), releasing total energy of 18.35 MeV. The fusion equation is expressed as [57]

$$\mathrm{D} + {}^3\mathrm{He} \rightarrow \mathrm{p}(14.68\mathrm{MeV}) + {}^4\mathrm{He}(3.67\mathrm{MeV}).$$

From the above two fusion reaction equations, it can be found that the energy released after D+T and D+He-3 reactions is approximately equivalent. Here, the energy released by tritium and helium-3 fuels as nuclear fusion reaction materials is discussed as follows.

The energy obtained by a specified mass of nuclear fuels during the nuclear fusion reaction can be calculated by the following equation:

$$P = \frac{M}{m} P_r \tag{6}$$

where M is the mass of nuclear fuels, and m is the atomic mass of nuclear fuels; P_r is the total energy produced.

1) The mass of one deuterium atomic and one tritium atomic is $\sim$2.014 u and $\sim$3.018 u, respectively. u is the atomic mass unit, 1.66×10^{-24} g; by substituting the above parameters into (6), the theoretical energy released by 1 g of tritium and deuterium is $\sim 2.11 \times 10^{24}$ MeV, corresponding to $\sim$337.12 GJ (1MeV $= 1.6 \times 10^{-13}$J).
2) The mass of one deuterium atomic and one helium-3 atomic is $\sim$2.014 u and $\sim$3.016 u, respectively; by substituting the above parameters into (6), the theoretical energy released by 1 g of the helium-3 and the deuterium is 2.20×10^{24} MeV, corresponding to $\sim$351.63 GJ.

The energy released by 1 g of D+T and 1 g of D+He-3 fuels is ∼81 tons and 84 tons of TNT, respectively, where the TNT equivalent is 4.184 GJ [58]. We do not need to worry about the reservoir of deuterium because it can be produced from seawater, and its total storage is about tens of trillion tons on Earth [59]. The same mass tritium and the helium-3 fuel release almost equivalent energy; therefore, we suggest that helium-3 may be a reasonable substitute for tritium as a nuclear fusion fuel. Compared with tritium for nuclear fusion, helium-3 has the following advantages in brief.

1) The cost of exploiting helium-3 on the Moon or Earth is lower than that of tritium.
2) The helium-3 reservoir on the Moon reaches one million tons.
3) A shortage of tritium.

However, it is worth noting that the use of helium-3 as a fuel for fusion is much more energy required than that of D+T fusion because of the coulomb barrier [60].

The cost of tritium on Earth is $30 000/g [56]. It is assumed that helium-3 is a substitute for tritium in the future and have the same price. The helium-3 price is at least three times higher than its cost of exploiting on the Moon, whose mining cost is $3850–$10 250/g. Therefore, it seems profitable to mine helium-3 resources from the lunar regolith on the Moon.

D. Proposal of Helium-3 Mining at the Chang'E-3 Landing Area

The Chang'E-3 landing area can be treated as a potential preselection area for future lunar helium-3 mining, it has the following advantages.

1) Assuming that the thickness of regolith per unit area of the Chang'E-3 is ∼9.24 m, the upper limit of the estimated helium-3 reservoir with ∼445 m ^{2} of the Chang'E-3 landing site is ∼84 g (the per unit area is ∼0.190 g/m^2), and the lower limit is ∼62 g (the per unit area is ∼0.138 g/m^2). The production of 2.0 tons of the helium-3 per year only requires the exploitation of regolith with an area of ∼10–15 km^2 at the Chang'E-3 landing site.
2) The Chang'E-3 landing area was located northeast of Mare Imbrium on the near side of the Moon, which is convenient for transportation between Earth and the Moon [61]. The geography of the landing area is relatively flat, with a slope of less than 15° [62], which is convenient for the construction of mining bases and the deployment of mining machines.
3) The landing area has been studied in detail by the Chang'E-3 mission [23], [62], [63].

In addition, commercial mining activities can also be considered to cooperate with scientific research to reduce the cost, e.g., building radar antenna systems for Moon-based Earth observation [64], lunar research laboratories, and Moon-based astronomical telescope platforms [65]. However, the feasibility of in-situ helium-3 mining on the Moon still faces great challenges, which are as follows.

1) Technical feasibility. Many countries have explored the Moon and realized the landing exploration of automatic robots and astronauts (e.g., the United States, the former Soviet Union, and China). The current technology has no difficulty in deploying mining machines on the Moon, but it still needs the research and development of automatic machines and equipment, which is suitable for working in the lunar environment.
2) Scientific feasibility. The estimated helium-3 reservoir on the global Moon is over one million tons [11]. Our result suggests that the reservoir of in-situ helium-3 resources may be underestimated.
3) Economic feasibility. The mining cost of lunar helium-3 is less than its economic value, but the transportation cost between Earth and the Moon is still very expensive. For example, NASA estimates that the cost price of returning 1 kg of material from the lunar surface is between $10 000 and $28 000 [55]. In addition, the complete scheme and cost budget of the lunar helium-3 mining system needs to be further improved.
4) Space policy feasibility. There is no consensus space policy for the exploitation of lunar minerals, currently. To reasonable utilization of lunar resources in the future, promoting the consensus on outer space behavior will also be beneficial to the exploitation of the Moon.
5) Moral feasibility. The exploitation of lunar helium-3 is bound to permanently change the geomorphological features of the Moon's surface, which may lead to moral and ethical disputes [66]. Especially, with the exploitation of helium-3 on the nearside of the Moon, the changed geomorphological features will be directly observed by optical telescopes on Earth. Therefore, before exploiting lunar minerals (not limited to the exploitation of helium-3), it is also necessary to reach a consensus on the exploitation of lunar resources. It is inevitable to change the geomorphological features of the Moon's surface during exploiting of the lunar helium-3 resources. The development and progress of human society is also a process of transforming the natural features of our Earth. We need to find a balance between transforming the geomorphological features and reducing the damage to the natural environment of the Moon.

In addition, the thickness of the regolith is unevenly distributed over the whole Moon [44]. Two high-precision in-situ radars measurement on the Moon suggest that the thickness of regolith is >10 m, e.g., Chang'E-3 and Chang'E-4 sites [26], [67], [68], [69], indicating that the global thickness of regolith is likely to be underestimated.

As the candidate raw material for nuclear fusion, helium-3 has many advantages, e.g., the nuclear fusion of D+He-3 reaction is one deuterium and one helium-3 to form one helium-4, one proton, and then release energy. The production of helium-3 nuclear fusion has no activated materials, which is friendly to the environment. In the D+T reaction, they form a helium-4, a neutron, and then release energy [70]. One of the problems associated with the D+T fusion reaction that produces neutrons is the activation of the walls of the reactor. So, it may be led the radiological risk.

Although the controller nuclear fusion technology is still under the research and development stage, its long-term feasibility and possible economic benefits are enticing. Once the controller

nuclear fusion technology is mature, its miniaturized equipment can be used as a power supply for variable vehicles, e.g., cars, ships, and even airplanes [71]. The helium-3 material can also be used in gas counters of neutron detectors and national defense security monitoring [72]. We predict that controllable nuclear fusion based on the helium-3 fuel becomes the mainstream of the nuclear power plant in the future, and this may change the current world's energy structure.

V. Conclusion

In summary, the Chang'E-3 high-frequency radar provides an opportunity to measure the thickness of the regolith with high accuracy and in-situ estimate its internal helium-3 reservoir. This study draws the following conclusions.

1) The Chang'E-3 high-frequency radar can be used to indirectly estimate the in-situ helium-3 reservoir in the lunar regolith.
2) Without considering the underestimation of the helium-3 concentration in the lunar regolith, the helium-3 reservoir in the area of $\sim$445 m^2 regolith (its thickness of $\sim$9.24 m) is estimated to be $\sim$37–51 g, and its corresponding helium-3 content per unit area is $\sim$0.083–0.114 g/m^2, which is at least five times higher than that of the global average.
3) It is expected that the lunar helium-3 to replace tritium as a nuclear fusion fuel is a possibility.
4) The exploitation of the lunar helium-3 seems to be profitable.
5) The Chang'E-3 landing area can be considered as a potential site selection for the exploitation of the lunar helium-3 in the future.

Above all, we suggest that mining the in-situ helium-3 resources on the Moon's surface seemingly has a considerable output–income ratio and economic benefits return, which might be one of the effective and feasible solutions to solve the future shortage of energy on Earth. Our results will provide a valuable reference to evaluate the economics and feasibility of mining in-situ helium-3 resources on the Moon.

Acknowledgment

The authors would like to thank the Ground Application System of Lunar Exploration, National Astronomical Observatories, Chinese Academy of Sciences, for providing the Moon-based GPR data used in this study, which are available at http://www.dx.doi.org/10.12350/CLPDS.GRAS.CE3.LPR-2B.vA.

References

[1] G. H. Heiken, D. T. Vaniman, and B. M. French, Eds., *Lunar Sourcebook, A User's Guide to the Moon*. Cambridge, U.K.: Cambridge Univ. Press, 1991.
[2] S. R. Taylor, *Planetary Science: A Lunar Perspective*, vol. 3303. Houston, TX, USA: Lunar Planet. Inst., 1982.
[3] C. Ding et al., "A review of applications of radar-detection techniques in lunar explorations," *Astronomical Res. Technol.*, vol. 12, no. 2, pp. 228–242, 2015.
[4] H. H. Schmitt and N. Armstrong, *Return to the Moon: Exploration, Enterprise, and Energy in the Human Settlement of Space*. Berlin, Germany: Springer, 2006.
[5] S. R. Taylor, G. J. Taylor, and L. A. Taylor, "The Moon: A Taylor perspective," *Geochimica et Cosmochimica Acta*, vol. 70, no. 24, pp. 5904–5918, 2006.
[6] L. Xu, Y. Zou, and J. Liu, "Helium-3 in lunar regolith," *Acta Mineralogica Sinica*, vol. 23, no. 4, pp. 374–378, 2003.
[7] P. H. Warren and J. T. Wasson, "The origin of KREEP," *Rev. Geophys.*, vol. 17, no. 1, pp. 73–88, 1979.
[8] H. H. Schmitt, "Mining the Moon," *Popular Mechanics*, vol. 12, pp. 58–61, 2004.
[9] J. R. Johnson, T. D. Swindle, and P. G. Lucey, "Estimated solar wind-implanted helium-3 distribution on the Moon," *Geophys. Res. Lett.*, vol. 26, no. 3, pp. 385–388, 1999.
[10] L. Taylor and G. Kulcinski, "Helium-3 on the Moon for fusion energy: The Persian Gulf of the 21st century," *Sol. Syst. Res.*, vol. 33, 1999, Art. no. 338.
[11] W. Fa and Y.-Q. Jin, "Quantitative estimation of helium-3 spatial distribution in the lunar regolith layer," *Icarus*, vol. 190, no. 1, pp. 15–23, 2007.
[12] S. Shukla, V. Tolpekin, S. Kumar, and A. Stein, "Investigating the retention of solar wind implanted helium-3 on the Moon from the analysis of multi-wavelength remote sensing data," *Remote Sens.*, vol. 12, no. 20, 2020, Art. no. 3350.
[13] C. Y. Ding, Z. Y. Xiao, Y. Su, J. N. Zhao, and J. Cui, "Compositional variations along the route of Chang'E-3 Yutu rover revealed by the lunar penetrating radar," *Prog. Earth Planet. Sci.*, vol. 7, no. 1, 2020, Art. no. 32.
[14] T. D. Swindle, C. E. Glass, and M. M. Poulton, "Mining lunar soils for 3He," UA/NASA Space Eng. Res. Center Utilization Local Planet. Resour., Univ. Arizona Press, Tech. Memorandum TM-90/1, 1990.
[15] I. A. Crawford, "Lunar resources: A review," *Prog. Phys. Geogr.*, vol. 39, no. 2, pp. 137–167, 2015.
[16] A. Murali and J. Jordan, "Helium-3 inventory of lunar samples: A potential future energy resource for mankind?," in *Proc. 24th Lunar Planet. Sci. Conf.*, vol. 24, 1993, pp. 1023–1024.
[17] R. B. Bilder, "A legal regime for the mining of helium-3 on the Moon: US policy options," *Fordham Interna Law J.*, vol. 33, pp. 243–257, 2009.
[18] W. Fa and Y. Jin, "Global inventory of helium-3 in lunar regoliths estimated by a multi-channel microwave radiometer on the Chang-E 1 lunar satellite," *Chin. Sci. Bull.*, vol. 55, no. 35, pp. 4005–4009, 2010.
[19] T. Simko and M. Gray, "Lunar helium-3 fuel for nuclear fusion: Technology, economics, and resources," *World Future Rev.*, vol. 6, no. 2, pp. 158–171, 2014.
[20] S. Matar, "Energy analysis of extracting helium-3 from the Moon," Ph.D. dissertation, Dept. Environ., Land Infrastructure Eng., Polytechnic Univ. Turin, Turin, Italy, 2021.
[21] C. Ding et al., "Layering structures in the porous material beneath the Chang'E-3 landing site," *Earth Space Sci.*, vol. 7, no. 10, 2020, Art. no. e2019EA000862.
[22] C. Ding, Z. Xiao, Y. Su, and J. Cui, "Hyperbolic reflectors determined from peak echoes of ground penetrating radar," *Icarus*, vol. 358, 2021, Art. no. 114280.
[23] L. Xiao et al., "A young multilayered terrane of the northern Mare Imbrium revealed by Chang'E-3 mission," *Science*, vol. 347, no. 6227, pp. 1226–1229, 2015.
[24] J. Zhang et al., "Volcanic history of the Imbrium basin: A close-up view from the lunar rover Yutu," *Proc. Nat. Acad. Sci. USA*, vol. 112, no. 17, pp. 5342–5347, 2015.
[25] Y. Su et al., "Data processing and initial results of Chang'E-3 lunar penetrating radar," *Res. Astron. Astrophys.*, vol. 14, no. 12, pp. 1623–1632, 2014.
[26] W. Fa, M. H. Zhu, T. T. Liu, and J. B. Plescia, "Regolith stratigraphy at the Chang'E-3 landing site as seen by lunar penetrating radar," *Geophys. Res. Lett.*, vol. 42, no. 23, pp. 10179–10187, 2015.
[27] L. Qiao, Z. Xiao, J. Zhao, and L. Xiao, "Subsurface structures at the Chang'E-3 landing site: Interpretations from orbital and in-situ imagery data," *J. Earth Sci.*, vol. 27, no. 4, pp. 707–715, 2016.
[28] J. Feng, Y. Su, C. Ding, S. Xing, S. Dai, and Y. Zou, "Dielectric properties estimation of the lunar regolith at CE-3 landing site using lunar penetrating radar data," *Icarus*, vol. 284, pp. 424–430, 2017.
[29] G. Y. Fang et al., "Lunar penetrating radar onboard the Chang'E-3 mission," *Res. Astron. Astrophys.*, vol. 14, no. 12, pp. 1607–1622, 2014.
[30] S.-G. Xing et al., "The penetrating depth analysis of lunar penetrating radar onboard Chang'E-3 rover," *Res. Astron. Astrophys.*, vol. 17, no. 5, 2017, Art. no. 046.
[31] H. B. Zhang et al., "Performance evaluation of lunar penetrating radar onboard the rover of CE-3 probe based on results from ground experiments," *Res. Astron. Astrophys.*, vol. 14, no. 12, pp. 1633–1641, 2014.

[32] C. Ding et al., "Rock fragments in shallow lunar regolith: Constraints by the lunar penetrating radar onboard the Chang'E4 mission," *J. Geophys. Res.: Planets*, vol. 126, no. 9, 2021, Art. no. e06917.
[33] C. Li et al., "Pitfalls in GPR data interpretation: False reflectors detected in lunar radar cross sections by Chang'E-3," *IEEE Trans. Geosci. Remote Sens.*, vol. 56, no. 3, pp. 1325–1335, Mar. 2018.
[34] D. S. McKay et al., "The lunar regolith," in *Lunar Sourcebook*. Cambridge, U.K.: Cambridge Univ. Press, 1991, pp. 285–356.
[35] M. Loeffler, C. Dukes, and R. Baragiola, "Irradiation of olivine by 4 keV He^+: Simulation of space weathering by the solar wind," *J. Geophys. Res.: Planets*, vol. 114, no. E3, 2009, Art. no. E03003.
[36] H. Song et al., "Theoretical study on thermal release of helium-3 in lunar ilmenite," *Minerals*, vol. 11, no. 3, 2021, Art. no. 319.
[37] S. Shukla, "Lunar regolith characterization for solar wind implanted helium-3 using M3 spectroscopy and biastatic miniature radar," Master's thesis, Geo-inf. Sci. Earth Observ., Univ. Twente, Enschede, The Netherlands, 2019.
[38] L. A. Taylor, "Helium-3 on the Moon: Model assumptions and abundances," in *Engineering, Construction, and Operations in Space IV*. Reston, VA, USA: ASCE, 1994, pp. 678–686.
[39] J. Arnold, "Monte Carlo simulation of turnover processes in the lunar regolith," in *Proc. Lunar Planet. Sci. Conf.*, 1975, pp. 2375–2395.
[40] V. L. Sharpton, "Outcrops on lunar crater rims: Implications for rim construction mechanisms, ejecta volumes and excavation depths," *J. Geophys. Res.: Planets*, vol. 119, no. 1, pp. 154–168, 2014.
[41] H. J. Melosh, *Impact Cratering: A Geologic Process*. New York, NY, USA: Oxford Univ. Press, 1989.
[42] W. Fa, T. Liu, M.-H. Zhu, and J. Haruyama, "Regolith thickness over Sinus Iridum: Results from morphology and size-frequency distribution of small impact craters," *J. Geophys. Res.: Planets*, vol. 119, no. 8, pp. 1914–1935, 2014.
[43] C. Ding et al., "Electromagnetic signal attenuation characteristics in the lunar regolith observed by the lunar regolith penetrating radar (LRPR) onboard the Chang'E-5 lander," *Remote Sens.*, vol. 14, no. 20, 2022, Art. no. 5189.
[44] Y. G. Shkuratov and N. V. Bondarenko, "Regolith layer thickness mapping of the Moon by radar and optical data," *Icarus*, vol. 149, no. 2, pp. 329–338, 2001.
[45] R. Sibson, "A brief description of natural neighbour interpolation," in *Interpreting Multivariate Data*. Hoboken, NJ, USA: Wiley, 1981, pp. 21–26.
[46] A. T. Basilevsky, A. M. Abdrakhimov, J. W. Head, C. M. Pieters, Y. Wu, and L. Xiao, "Geologic characteristics of the Luna 17/Lunokhod 1 and Chang'E-3/Yutu landing sites, Northwest Mare Imbrium of the Moon," *Planet. Space Sci.*, vol. 117, pp. 385–400, 2015.
[47] Z. Ling et al., "Correlated compositional and mineralogical investigations at the Chang'E-3 landing site," *Nature Commun.*, vol. 6, no. 1, pp. 1–9, 2015.
[48] J. Mitchell et al., "Mechanical properties of lunar soil: Density, porosity, cohesion and angle of internal friction," in *Lunar Planet. Sci. Conf. Proc.*, vol. 3, 1972, Art. no. 3235.
[49] W. D. Carrier, III, G. R. Olhoeft, and W. Mendell, "Physical properties of the lunar surface," in *Lunar Sourcebook*. Cambridge, U.K.: Cambridge Univ. Press, 1991, pp. 475–594.
[50] G. R. Olhoeft and D. Strangway, "Dielectric properties of the first 100 meters of the Moon," *Earth Planet. Sci. Lett.*, vol. 24, no. 3, pp. 394–404, 1975.
[51] L. Sun et al., "Lunar iron and optical maturity mapping: Results from partial least squares modeling of Chang'E-1 IIM data," *Icarus*, vol. 280, pp. 183–198, 2016.
[52] J. S. Lewis, "Extraterrestrial sources of 3He for fusion power," *Space Power*, vol. 10, no. 3/4, pp. 363–372, 1991.
[53] S. Dobransky, "Helium-3: The future of energy security," *Int. J. World Peace*, vol. 30, no. 1, pp. 61–88, 2013.
[54] A. Kleinschneider et al., "Feasibility of lunar Helium-3 mining," in *Proc. 40th COSPAR Sci. Assem.*, vol. 40, 2014, pp. B0.1–58-14.
[55] J. Niechciał et al., "Operational costs of He3 separation using the superfluidity of He4," *Energies*, vol. 13, no. 22, 2020, Art. no. 6134.
[56] D. Clery, "Out of gas—A shortage of tritium fuel may leave fusion energy with an empty tank," *Science*, vol. 376, pp. 1372–1376, 2022.
[57] R. V. Petrescu, R. Aversa, S. Kozaitis, A. Apicella, and F. I. Petrescu, "Some proposed solutions to achieve nuclear fusion," *Amer. J. Eng. Appl. Sci.*, vol. 10, no. 3, pp. 703–708, 2017.
[58] S. Sahin, R. W. Moir, A. Şahinaslan, and H. M. Şahin, "Radiation damage in liquid-protected first-wall materials for IFE-reactors," *Fusion Technol.*, vol. 30, no. 3P2A, pp. 1027–1035, 1996.
[59] C. Rüth, "Harnessing the power of the sun: Fusion reactors," *Sci. Sch.*, vol. 22, pp. 42–48, 2012.
[60] J. Bahmani, "The feasibility of using 3He-3He fuel in a fusion reactor," *J. Nucl. Sci.*, vol. 6, no. 1, pp. 1–7, 2019.
[61] C. Ding et al., "Numerical simulations of the lunar penetrating radar and investigations of the geological structures of the lunar regolith layer at the Chang'E 3 landing site," *Int. J. Antennas Propag.*, vol. 2017, pp. 1–11, 2017.
[62] B. Wu et al., "Topographic modeling and analysis of the landing site of Chang'E-3 on the Moon," *Earth Planet. Sci. Lett.*, vol. 405, pp. 257–273, 2014.
[63] C. Ding, Y. Cai, Z. Xiao, and Y. Su, "A rocky hill on the continuous ejecta of Ziwei crater revealed by the Chang'E-3 mission," *Earth Planet. Phys.*, vol. 4, no. 2, pp. 105–110, 2020.
[64] H. Guo, G. Liu, and Y. Ding, "Moon-based Earth observation: Scientific concept and potential applications," *Int. J. Digit. Earth*, vol. 11, no. 6, pp. 546–557, 2018.
[65] W. Duan, S. Huang, and C. Nie, "Entrance pupil irradiance estimating model for a Moon-based Earth radiation observatory instrument," *Remote Sens.*, vol. 11, no. 5, 2019, Art. no. 583.
[66] D. Capper, "What should we do with our Moon?: Ethics and policy for establishing international multiuse lunar land reserves," *Space Policy*, vol. 59, 2022, Art. no. 101462.
[67] C. L. Li et al., "The Moon's farside shallow subsurface structure unveiled by Chang'E-4 lunar penetrating radar," *Sci. Adv.*, vol. 6, no. 9, 2020, Art. no. eaay6898.
[68] C. Ding et al., "Fragments delivered by secondary craters at the Chang'E4 landing site," *Geophys. Res. Lett.*, vol. 47, no. 7, 2020, Art. no. e2020GL087361.
[69] R. Wang et al., "A novel approach for permittivity estimation of lunar regolith using the lunar penetrating radar onboard Chang'E-4 rover," *Remote Sens.*, vol. 13, no. 18, 2021, Art. no. 3679.
[70] G. L. Kulcinski and H. H. Schmitt, "Nuclear power without radioactive waste—The promise of lunar helium-3," *Moon*, vol. 2, pp. 20–21, 2000.
[71] R. V. V. Petrescu, A. Machin, K. Fontanez, J. C. Arango, F. M. Marquez, and F. I. T. Petrescu, "Hydrogen for aircraft power and propulsion," *Int. J. Hydrogen Energy*, vol. 45, no. 41, pp. 20740–20764, 2020.
[72] R. T. Kouzes, A. T. Lintereur, and E. R. Siciliano, "Progress in alternative neutron detection to address the helium-3 shortage," *Nucl. Instrum. Methods Phys. Res. Sect. A: Accel., Spectrometers, Detect. Assoc. Equip.*, vol. 784, pp. 172–175, 2015.

Chunyu Ding received the Ph.D. degree in astronomy from the University of Chinese Academy of Sciences, Beijing, China, in 2017.

He has been an Assistant Professor with the Institute of Advance Study, Shenzhen University, Shenzhen, China, since 2021. He is a Core Scientific Member of the Chinese Chang'E-4 Mission and also involves in the team on the radar group of the Chinese First Mars Mission, Tianwen-1. His research interests include the radar detection of terrestrial planets and the surface evolution of terrestrial bodies in the solar system, e.g., the Moon and Mars.

Qingquan Li received the Ph.D. degree in geographic information system and photogrammetry from the Wuhan Technical University of Surveying and Mapping, Wuhan, China, in 1998.

From 1988 to 1996, he was an Assistant Professor with Wuhan University, Wuhan, where he became an Associate Professor in 1996 and has been a Professor since 1998. He is currently a Professor with Shenzhen University, Shenzhen, China, and the State Key Laboratory of Information Engineering in Surveying, Mapping and Remote Sensing, Wuhan University, where he is also the Director of the Shenzhen Key Laboratory of Spatial Smart Sensing and Service. His research interests include intelligent transportation systems, 3-D and dynamic data modeling, and pattern recognition.

Dr. Li is an Academician of the International Academy of Sciences for Europe and Asia (IASEA), an Expert in Modern Traffic with the National 863 Plan, and an Editorial Board Member of the *Journal of Surveying and Mapping* and the Wuhan University Journal—*Information Science* Edition.

Jiangwan Xu received the bachelor's degree of engineering degree in civil engineering from the College of Civil Engineering and Transportation Engineering, Shenzhen University, Shenzhen, China, in 2020. He is currently working toward the master's degree in civil engineering with Shenzhen University, Shenzhen, China.

His main research interests include development, utilization, and evaluation of geothermal resources.

Zhonghan Lei received the degree from the Institute of Advanced Research, Shenzhen University, Shenzhen, China, in 2019. He is currently working toward the bachelor's degree in physics with Shenzhen University, Shenzhen, China.

His main research interests include data processing and interpretation of Chang'E-4 ground penetrating radar.

Jiawei Li received the Ph.D. degree in astronomy from the University of Chinese Academy of Sciences, Beijing, China, in 2020.

His main research interests include management and distribution of planetary exploration data.

Yan Su received the Ph.D. degree in astronomical techniques and methodology from the National Astronomical Observatories, Chinese Academy of Sciences (CAS), Beijing, China, and The University of Manchester, Manchester, U.K., in 2003, under the Joint Doctoral Program.

Since 2012, she has been a Professor with the National Astronomical Observatories, CAS. Her research interests include ground-penetrating radar data processing and interpretation, developing the downlink ground stations for Chinese deep space exploration, and microwave radiometer applications for planetary investigations.

Shaopeng Huang received the Ph.D. degree in geology from the Institute of Geology, Chinese Academy of Sciences, Beijing, China, in 1990.

He was the Chairman of the International Heat Flow Commission (IHFC) of the International Association of Seismology and Geophysics of the Earth Interior (IASPEI) from 2015 to 2019 and has authored or coauthored more than 100 influential papers, including *Nature*, *Science*, *Nature Climate Change*, and *Science Bulletin*.

Dr. Huang was selected into the Hundred Talents Program of the Chinese Academy of Sciences in 2008 and was selected as a distinguished expert of Shaanxi Province in 2011.